International Journal of Bioelectromagnetism
Vol. 13, No. 4, pp. 261-267, 2011

ESI and fMRI of interictal and ictal epileptic discharges

Simon Vogrin[a,b], Stephan Lau[a,b,c], Mark Cook[a,b], Jens Haueisen[c]
[a]*Centre for Clinical Neurosciences and Neurological Research, St. Vincent's Hospital Melbourne, AUSTRALIA*
[b]*Neuroengineering Group, Dept. of Electrical and Electronic Engineering, The University of Melbourne, AUSTRALIA*
[c]*Institute of Biomedical Engineering and Informatics, Ilmenau Technical University, GERMANY*
Correspondence: S. Vogrin, Centre for Clinical Neurosciences and Neurological Research, St. Vincent's Hospital Melbourne
E-mail: simon.vogrin@svhm.org.au, phone +61 3 92883653

Abstract. A major challenge in planning and performing resective surgery in drug-resistant epilepsy is the accurate identification of the epileptogenic zone. Currently, intracranial EEG is considered to be the most reliable preresective functional localisation method. Our objective is to non-invasively localise the epileptogenic zone using simultaneous high-density EEG source imaging (ESI) and fMRI of interictal and ictal discharges. We performed two 128-channel EEG recordings, in a shielded room and simultaneous EEG-fMRI, of a focal epilepsy patient in a single session and captured interictal discharges and one seizure exhibiting oscillatory activity of 14 Hz. The locations described by fMRI and ESI of interictal events in the MR scanner and shielded room show good anatomical agreement with each other; the ictal ESI; and with video EEG monitoring, PET and ictal SPECT. Averaging of ictal oscillatory periods strengthens the localisation, while the quantity of concordant interictal events supports reliability of interictal localisations. Simultaneous high-density EEG and fMRI acquisition non-invasively provides added localising information in a multimodal context. Concordant simultaneous ESI and fMRI localisation of interictal and ictal events shows promise in improving non-invasive presurgical evaluation of epilepsy.

Keywords: Electrical source imaging; Dipole; BOLD effect; Epileptic seizure; Interictal discharge; Presurgical planning; Focal epilepsy

1. Introduction

A major challenge in planning and performing resective surgery in drug-resistant epilepsy is the accurate identification of the epileptogenic zone. Currently, intracranial EEG is considered to be the most reliable preresective functional localisation method [Leeman et al., 2008]. Our objective is to non-invasively localise the epileptogenic zone using simultaneous high-density EEG source imaging (ESI) and fMRI of interictal and ictal discharges.

2. Material and Methods

2.1. Clinical Case

A patient with intractable MRI-negative focal epilepsy volunteered to participate. The patient presented with stereotyped seizure semiology including hand and chewing automatisms with a distinct vocalization. Seizures and interictal events were very frequent; multiple per day. In-patient Video-EEG monitoring demonstrated frequent left temporal sharp interictal activity (F7/T3). Recorded seizures were often characterized by a 14Hz rhythm. PET scans were reported to show clear left temporal hypometabolism, while SPECT imaging showed no definite ictal focus and normal cerebral perfusion.

2.2. EEG/fMRI and EEG Measurements

We recorded the EEG of the patient with a 128 channel cap at 10kHz simultaneously to fMRI to capture interictal epileptic discharges (IEDs). A second EEG recording with the same equipment was performed in a shielded room immediately after the EEG-fMRI recording. In both recordings, frequent IEDs were observed, as well as a seizure in the shielded room. EPI artefacts in the EEG were removed with average artefact subtraction [Allen et al., 2000]. The ballistocardiogram (BCG) was removed using PCA projection.

2.3. Electrical Source Imaging

A patient-specific realistic boundary element model (skin, skull and brain) was constructed from a 1mm isotropic MPRAGE image. The electrode positions were derived from a second MPRAGE image made while the patient was wearing the cap. Results from fMRI analyses were imported into the study to improve comparisons in the common solution space of the MPRAGE volume. A cortically constrained current density source model (sLORETA) as well as a moving dipole fit were applied to individual IEDs, averaged IEDs and the seizure using Curry 6.0.16 (Compumedics Neuroscan, Hamburg, Germany).

2.4. MR Acquisition & Analysis

Subject was scanned on a 1.5T Avanto TIM MR scanner (Siemens, Erlangen, Germany) with 12-channel phased array head coil. All results were coregistered with the MPRAGE dataset (FOV) 25.6 × 25.6 cm^2, matrix 256 × 256 TR 2.5 s, TE 51 ms, flip angle 15°, 256 adjacent slices (1 mm isotropic volume). Functional MRI images were recorded for 35 minutes continuously with a T2*-weighted single shot spin echo-planar imaging (EPI) sequence: FOV = 24 × 24 cm^2, matrix 128 × 128, TR 3.0 s, TE 51 ms, flip angle 90°, 25 interleaved slices, with reconstructed voxel size 1.9 × 1.9 × 5 mm^3.

EEG activity was reviewed for interictal discharges following MR gradient artifact removal with Scan 4.5 (Compumedics Neuroscan, Charlotte North Carolina, USA) and ballistocardiogram effects by Curry 6 respectively (Compumedics Neuroscan, Hamburg Germany). Timing of events was recorded from the start of the first fMRI volume. Eleven IEDs were chosen as event times for the design matrix primary regressor variable (including event duration and amplitude), and an additional four regressors modeled delays of 3.0s, 5.0s, 7.0s and 9.0s respectively. General Linear Model (GLM) analysis of the fMRI was performed by FSL FEAT toolbox (FMRIB Centre, University of Oxford, England) incorporating slice-timing and motion corrections, and a 6mm FWHM Gaussian smoothing kernel, while the interictal events were convolved with a canonical haemodynamic response function (HRF).

3. Results

3.1. Interictal Discharges

Source analysis located the peak of interictal discharges in the left medial temporal region (Fig. 1 middle column) with a distribution around the averaged IED of mean±SD = 13.8±7.9 mm (Table 1). Variation in the X dimension (left-right) was smaller than in Y (posterior-anterior) and Z (inferior-superior). The orientations of IEDs were consistent with distribution around the orientation of the averaged IED of mean±SD = 11.7±7.8° (Table 1).

Table 1. *Equivalent dipoles of interictal discharges and their variation in standardized coordinate system (X = left-right, Y = posterior-anterior , Z = inferior-superior) at the time of peak amplitude of the interictal discharge.*

#	*X [mm]*	*Y [mm]*	*Z [mm]*	*Deviation from average [mm]*	*nX*	*nY*	*nZ*	*Deviation from average [°]*
Mean	-34.6	17.4	50.6	13.8	-0.95	0.20	-0.13	11.7
SD	3.4	10.9	9.5	7.9	0.04	0.18	0.13	7.8
Averaged IED	-35.1	21.3	55.3	--	-0.94	0.29	-0.16	--

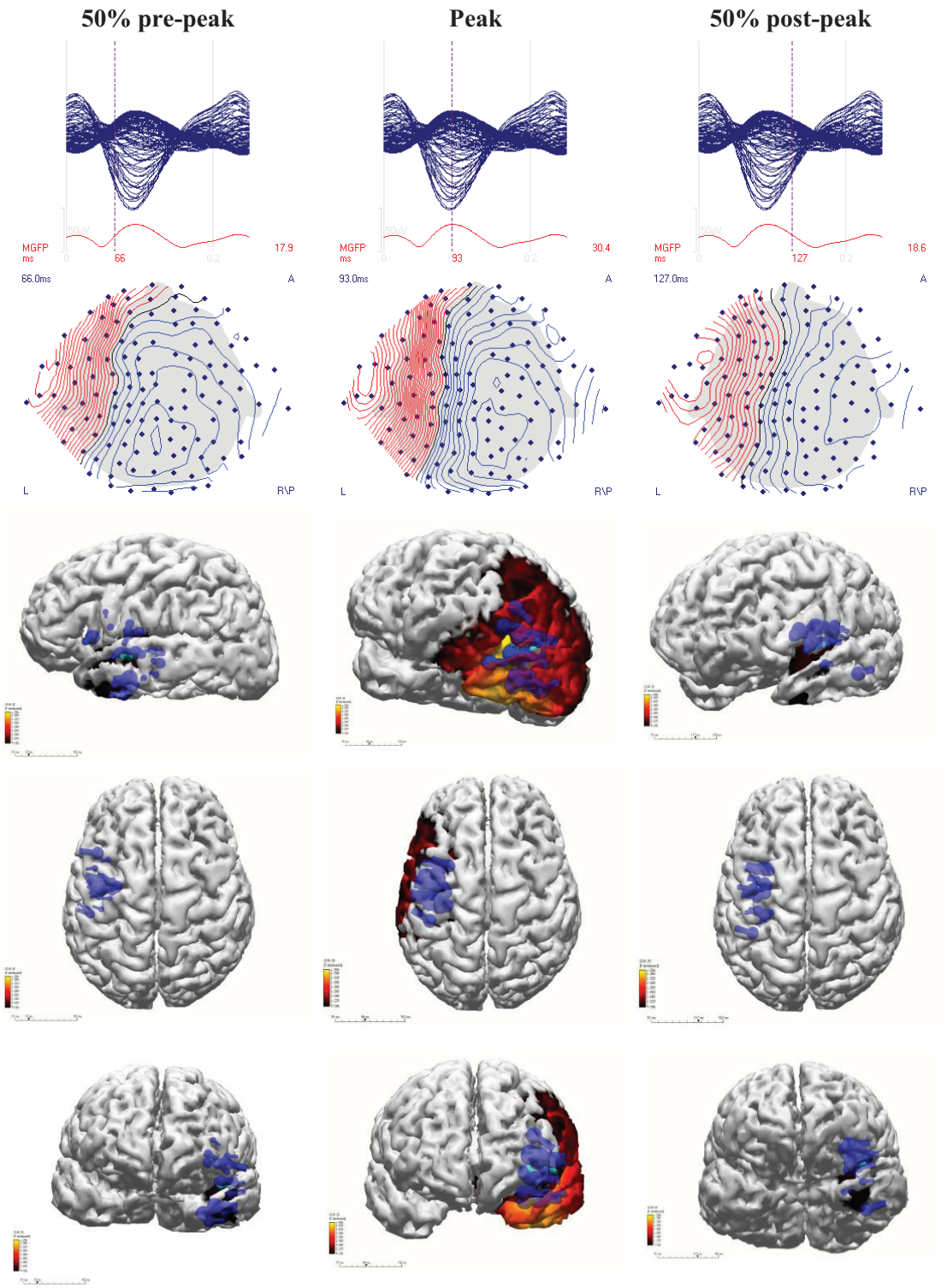

Figure 1. *Individual moving dipole fit of 23 interictal discharges (blue dipoles) at time points of 50% amplitude pre-peak (left column), peak (middle column) and 50% amplitude post-peak (right column) overlaid with a current density reconstruction and moving dipole fit (turquoise) of their average shown in three orientations (rows). Butterfly plots and potential maps (top row) are of the respective average.*

3.2. Ictal Discharge

The ictal event demonstrated a 14 Hz rhythm over 3 seconds (Fig. 2 top row). To isolate the 14 Hz rhythm, the EEG was bandpass filtered between 12 and 16 Hz. The average of 20 periods was located at the level of the middle-temporal gyrus (Fig. 2 right column). To assess the impact of additional frequencies, the EEG was filtered with 1-30 Hz and averaged over the same interval. This shifted the equivalent dipole location about 10 mm superiorly into the superior-temporal gyrus (Fig. 2 left column) and altered the orientation by 14º (Table 2).

Table 2. *Equivalent dipoles of averaged discharges and their deviation in standardized coordinate system (X = left-right, Y = posterior-anterior , Z = inferior-superior) at the time of peak amplitude respectively.*

Discharge	*X [mm]*	*Y [mm]*	*Z [mm]*	*Distance from ictal average (12-16 Hz) [mm]*	*nX*	*nY*	*nZ*	*Angular deviation from ictal average (12-16 Hz) [°]*
Ictal average (12-16 Hz)	-46.8	2.4	48.3	--	-0.98	0.02	0.18	--
Ictal average (1-30 Hz)	-45	-5.4	42.9	9.7	-0.94	0.25	0.25	14.0
Interictal average	-35.1	21.3	55.3	23.3	-0.94	0.29	-0.16	25.3
fMRI centre†	-54.4	30.3	46.5	29.0	--	--	--	--

†fMRI centre is centroid of closest neighbouring fMRI activation to ictal and interictal current dipole.

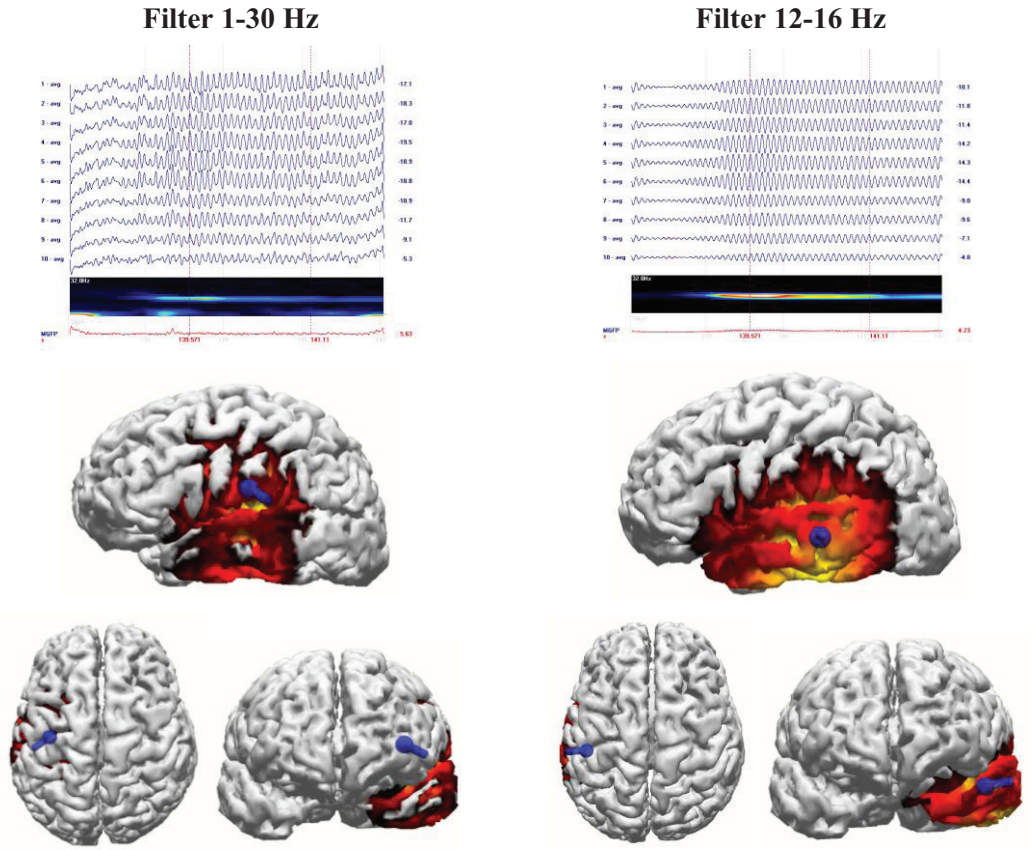

Figure 2. *Current density reconstruction and dipole fit the averaged (20x) ictal 14 Hz discharge filtered at 1-30 Hz (left) and 12-16 Hz (right) shown in three orientations (rows). Channel plots and potential maps (top row) are of the respective average.*

3.1. fMRI of interictal discharges

The fMRI analysis (Fig. 3 & 4) demonstrated two areas of activation concordant with seizure lateralisation based on seizure semiology. The hand automatisms considered to occur frequently with ictal events (right hand pointing) was seen to correlate to a BOLD response during modelling of the interictal discharges. The significance of the frontal activation contralateral remains unclear, although is likely to represent part of an extended network involved in the epileptic brain.

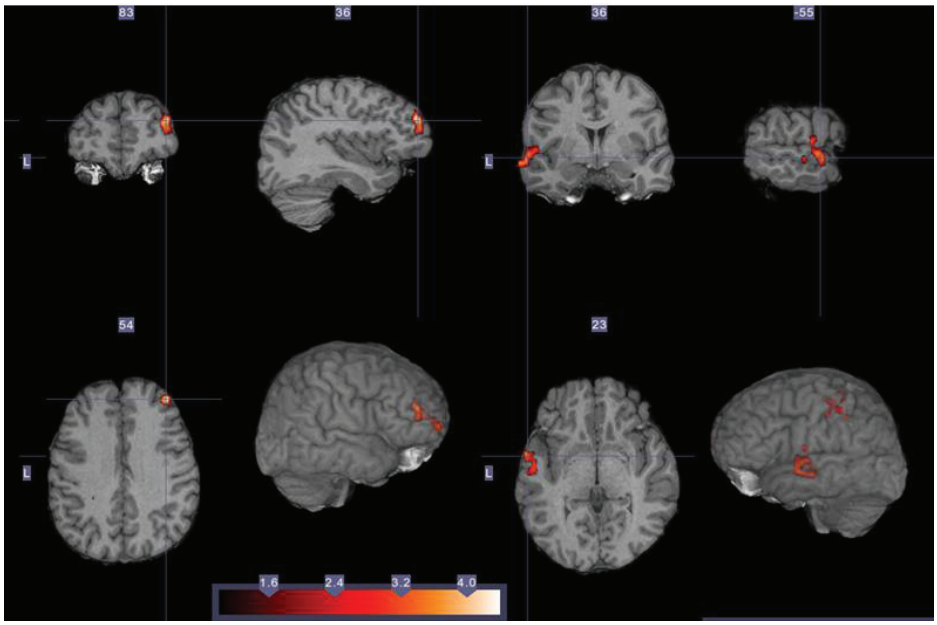

Figure 3. *fMRI localization of 11 interictal discharges over 35 minute simultaneous EEG-fMRI using a multi HRF approach. Three principle clusters were determined in the left superior temporal gyrus, right frontal and left precentral gyrus.*

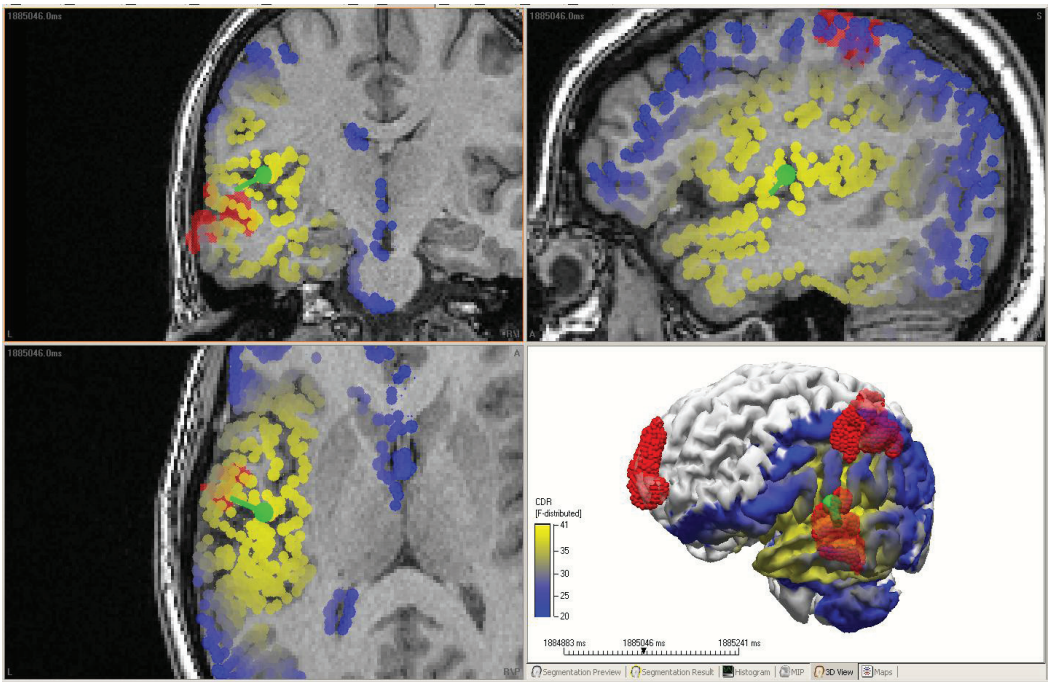

Figure 4. *ESI and fMRI colocalization of interictal discharges from simultaneous EEG-fMRI data. Cortically-constrained sLORETA used to determine the strength of distributed sources (blue-yellow scaled spheres) in the left superior temporal region,and equivalent moving current dipole (green). Sampled points within fMRI activations were represented as spheres (red).*

3.2.Channel density of interictal discharges

Localisation of interictal discharges were compared on the same dataset using 26, 58 and 120 channels respectively (Fig. 5.) The result of reduced channel density shows minor deviation from 58 to 120 channels; however a clear shift in position superiorly, and orientation laterally was evident from 26 channel dipole solution. All interictal reconstructions demonstrated clustering near the principal fMRI activation, but a consistent anterior shift from the reconstructed ictal (orange dipole) in posterior left middle temporal gyrus.

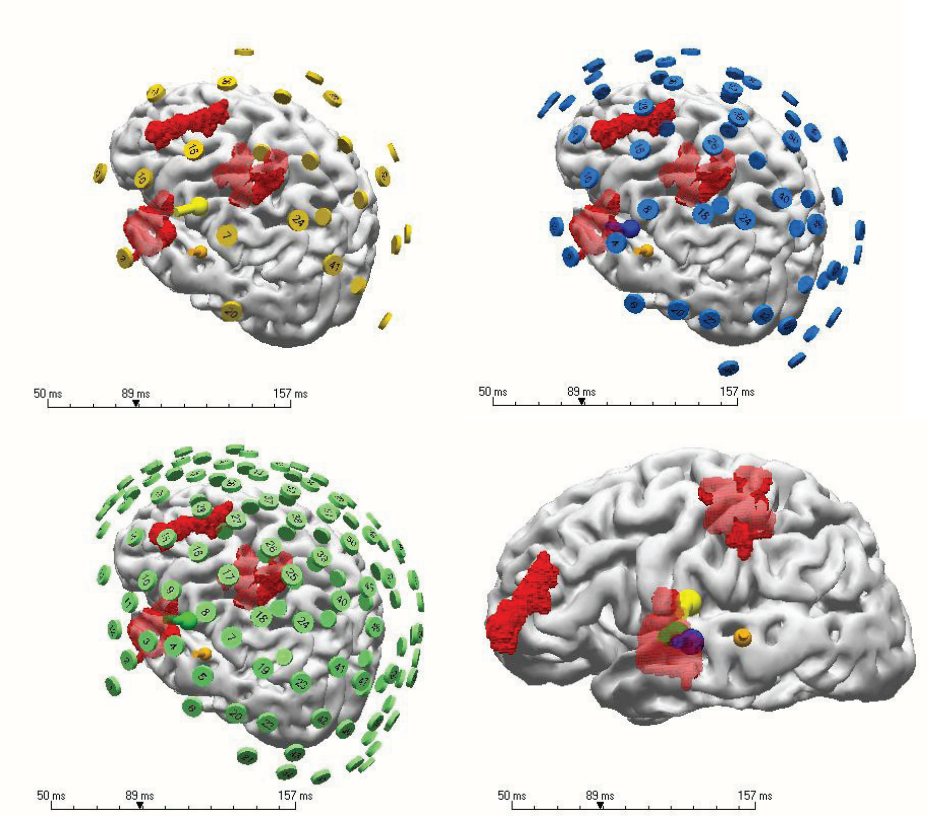

Figure 5. *Averaged CDR dipole fit of 23 interictal discharges recorded outside of the scanner. Spatially subsampled reconstructions at the earliest channel peak (89ms) show yellow dipole result from 26 channels represented as yellow electrodes (upper left,) and blue dipole from 58 channels from blue electrodes (upper right) with respect to complete 120 valid channels (green dipole and electrodes, lower left). The combined summary (lower right) demonstrates the consistency of the reconstructions proximal to interictal EEG-fMRI activation, but independent from recorded ictal event (orange dipole provided as reference in each image).*

4. Discussion

The locations described by fMRI and ESI of interictal events in the MR scanner compared with shielded room recordings show anatomical agreement with each other (Fig. 4); the ictal ESI (Fig. 3); and standard clinical investigations reported from video EEG monitoring, PET and ictal SPECT. Averaging of ictal oscillatory periods strengthens localisation of ictal sources, while the quantity of concordant IEDs supports reliability of the interictal localisations. Despite ESI having been successfully employed in other epilepsy studies along with EEG-fMRI [Siniatchkin et al. 2010; Groening et al. 2009; Vulliemoz et al., 2010], this study represents the first to directly examine source reconstruction of high channel density from 128 channels both inside and outside the MRI scanner.

Concordance in source reconstructions of interictal discharges (recorded both in- and outside of the MR scanner) within the same session reduces potential error introduced by variable electrode locations, allowing the yield of increased electrode density recording during simultaneous EEG-fMRI to be assessed directly. The rising slope versus peak of the individual interictal discharges showed a conservative angular distribution around the mean and a distance over 13 mm from the dipole reconstruction on the averaged interictal discharge from EEG data recorded in the shielded room.

Temporal filtering of the ictus between 12-16 Hz showed a 10 mm difference in position. However, distances from this interictal average to ictal events was similar to those between interictal and nearby centroid of fMRI activation (23 mm). The variability of source localisation is greater than current gold standard of 1cm when employing direct cortical stimulations with a probe in theatre, yet remains a likely non-invasive surrogate when comparing all increased risks. The potential for improved resolution between multiple "candidate" fMRI activations by using source reconstruction is evident [Vulliemoz et al., 2010], and the integration of multimodal model approaches available in theatre, highlight the need to select from either anatomical or functional, or spatial or temporal. Visually combined these can greatly enhance clinical utility [Plummer et. al., 2007; Murphy et al., 2004].

Residual noise after post-processing of the main EEG-fMRI induced artifacts is an error source that remains an area for development. The practical return for larger scale electrode coverage is justified by enhanced characterisation of interictal events outside of the scanner and further enable independent assessment of each high density ESI event for inclusion as an interictal fMRI regressor. The stability of the ESI solution is retained irrespective of whether individual EEG channels must later be omitted from analysis, ensuring the benefits of using ESI and individualised head models to assist in delineating between real and artifactual events. ESI modelling of interictal events alone may provide an incomplete representation of the ictal activation and/or epileptogenic regions involved, however their incorporation with simultaneous EEG-fMRI (despite additional acquisition and analysis time) remains a cheaper and safer option for resolving poorly localised epileptiform activity, especially when compared to other technologies employing radiotracer materials such as PET and SPECT.

5. Conclusions

Simultaneous high-density EEG and fMRI acquisition non-invasively provides added localising information in a multimodal context. Concordant simultaneous ESI and fMRI localisation of interictal and ictal events shows promise in improving non-invasive presurgical evaluation of epilepsy.

Acknowledgements

We wish to thank Wendyl D'Souza, Levin Kuhlmann, Mark Lourensz, Nicholas Trost, Emma Steele and The Bionic Ear Institute (Melbourne, Australia). This work has been supported by the Australian NHMRC, the German DFG, the German DAAD and the Australian Group of Eight.

References

Allen PJ, Josephs O, Turner R. A method for removing imaging artifact from continuous EEG recorded during functional MRI. *NeuroImage*, 12(2):230–239, 2000.

Bagshaw AP, Kobayashi E, et al. Correspondence between EEG-fMRI and EEG dipole localisation of interictal discharges in focal epilepsy. *NeuroImage* 30:417-425, 2005.

Groening K, Brodbeck V, Moeller F, Wolff S, van Baalen A, Michel CM, Jansen O, Boor R, Weigand G, Stephani U, Siniatchkin M. Combination of EEG-fMRI and EEG source analysis improves interpretation of spike-associated activation networks in pediatric pharmacoresistant focal epilepsies. *Neuroimage* 46(3): 827-833, 2009

Grova C, Daunizeau J, et al. Concordance between distributed EEG source localisation and simultaneous EEG-fMRI studies of epileptic spikes. *NeuroImage* 39:755-774, 2008.

Leeman BA, Cole AJ. Advancements in the Treatment of Epilepsy. *Annual Review of Medicine* 59: 503-523, 2008.

Murphy MA, O'Brien TJ, Morris K, Cook MJ. Multimodality Image-guided surgery for the treatment of medically refractory epilepsy. *J Neurosurgery* 100(3):452-62, 2004.

Nunez PL, Silberstein RB. On the relationship of synaptic activity to macroscopic measurements: Does co-registration of EEG with fMRI make sense? *Brain Topography* 13:79-96, 2000.

Plummer C, Litewka L, Farish S, Harvey AS, Cook MJ. Clinical utility of current-generation dipole modelling of scalp EEG. *Clinical Neurophysiology* 118(11):2344-61, 2007.

Salek-Haddadi A., Diehl, et al. Hemodynamic correlates of epileptiform discharges: An EEG-fMRI study of 63 patients with focal epilepsy. *Brain Research* 1088: 148-166, 2006.

Siniatchkin M, Groening K, Moehring J, Moeller F, Boor R, Brodbeck V, Michel CM, Rodionov R, Lemieux L, Stephani U. Neuronal networks in children with continuous spikes and waves during slow sleep. *Brain* 133; 2798-2813, 2010

Vulliemoz S, Rodionov R, Carmichael DW, Thornton R et al. Continuous EEG source imaging enhances analysis of EEG-fMRI in focal epilepsy. *NeuroImage*, 49:3219–3229, 2010.